International Journal of ENGINE RESEARCH

Standard Article

International J of Engine Research
2020, Vol. 21(3) 421–436

DOI: 10.1177/1468087418788491
journals.sagepub.com/home/jer
SAGE

Development and experimental validation of a real-time capable field programmable gate array–based gas exchange model for negative valve overlap

David Gordon[1], Christian Wouters[2], Maximilian Wick[3], Feihong Xia[3], Bastian Lehrheuer[4], Jakob Andert[3], Charles R Koch[1] and Stefan Pischinger[4]

Abstract

Homogeneous charge compression ignition has the potential to significantly reduce NO_x emissions, while maintaining a high fuel efficiency. Homogeneous charge compression ignition is characterized by compression-induced autoignition of a lean homogeneous air–fuel mixture. Combustion timing is highly dependent on the in-cylinder state including pressure, temperature and trapped mass. To control homogeneous charge compression ignition combustion, it is necessary to have an accurate representation of the gas exchange process. Currently, microprocessor-based engine control units require that the gas exchange process is linearized around a desired operating point to simplify the model for real-time implementation. This reduces the models' ability to handle disturbances and limits the flexibility of the model. However, using a field programmable gate array, a detailed simulation of the physical gas exchange process can be implemented in real time. This paper outlines the process of converting physical governing equations to an offline zero-dimensional gas exchange model. The process used to convert this model to a field programmable gate array capable model is described. This model is experimentally validated using a single cylinder research engine with electromagnetic valves to record real-time field programmable gate array gas exchange results and comparing to the offline zero-dimensional physical model. The field programmable gate array model is able to accurately calculate the cylinder temperature and cylinder mass at 0.1 °CA intervals during the gas exchange process for a range of negative valve overlaps, boost conditions and engine speeds making the model useful for future real-time control applications.

Keywords

Field programmable gate array, homogeneous charge compression ignition, gasoline-controlled autoignition, gas exchange model, zero-dimensional engine simulation

Date received: 2 February 2018; accepted: 10 June 2018

Introduction

Homogeneous charge compression ignition (HCCI) is a part-load combustion method, which is characterized by lean low-temperature combustion (LTC) with temperatures below the NO_x formation temperature of 2000 K. As a result, HCCI has the potential to significantly reduce NO_x emissions, while maintaining a high fuel efficiency, comparable with current stratified lean-burn combustion, with NO_x emissions reduced by up to 99%.[1–4] Therefore, expensive exhaust aftertreatment systems can be reduced or simplified.[4–6] Improved efficiency is also possible when using HCCI combustion

[1]Department of Mechanical Engineering, University of Alberta, Edmonton, AB, Canada
[2]Department of Mechanical Engineering, Eindhoven University of Technology, Eindhoven, Netherlands
[3]Mechatronic Systems for Combustion Engines, RWTH Aachen University, Aachen, Germany
[4]Institute for Combustion Engines, RWTH Aachen University, Aachen, Germany

Corresponding author:
David Gordon, Department of Mechanical Engineering, University of Alberta, Edmonton T6G 2R3, AB, Canada.
Email: dgordon@ualberta.ca

due to the rapid global and spatial combustion in combination with reduced wall heat losses from the LTC. The potential of HCCI combustion has been proven in numerous research projects.[4,7–11]

HCCI combustion is enabled by compression-induced autoignition, which is highly dependent on the cylinder state after compression. The lack of a direct combustion timing control method like ignition timing in spark ignition (SI) engines or injection timing in traditional compression ignition (CI) engines is a major disadvantage, which has caused a strong research focus on control strategies. Temperature has a large impact on ignition timing and can be altered through intake air heating, increased compression ratio or exhaust gas recirculation (EGR).[12–14] Using two fuels with different ignition properties changes the chemical composition of the cylinder and has also shown potential for HCCI control.[15–17]

Near the misfire limit, when using EGR as a means to provide the thermal energy required to achieve autoignition, a strong coupling between cycles can exist.[18] Consequently, the tendency for unstable combustion sequences increases, which proves to be problematic, especially during engine transients and near the misfire limit. Current cycle-based control strategies only stabilize a small portion of the operation range, which is insufficient for practical engine deployment.[19] For the extension of the operation range, use of external EGR and boosting was suggested.[20] Unfortunately, these measures yield reduced combustion stability, since the dependence of the combustion on boost pressure, EGR composition and maximum pressure gradient varies widely during the transient operation which can dilute the mixture, thus lowering the autoignition tendency. A stabilizing controller that works over a wide range of operating conditions is needed. Distinct cyclic variations, characterized by a spontaneous shift from stable to unstable operation, has been investigated in the literature.[4,21–26]

To develop a deeper understanding of HCCI combustion, simulation models have been developed to predict the gas exchange and combustion processes. These include stochastic, multi-zone and physical models. Generally, detailed physical models are computationally too intensive for use in real-time engine applications and are linearized around a specific operating point.[27,28] For their use in real-time applications, it is necessary to relinearize the model for different operating points. A physics-based, zero-dimensional (0D) model is described in the first part of this article and is useful for determining the in-cylinder state during the entire gas exchange process. This information is often desired for HCCI combustion controllers as an input.

For complex cylinder pressure analysis and control algorithms in real time, the low latency and parallel computing architecture of field programmable gate array (FPGA) hardware are useful.[29] FPGA hardware has successfully been used in experimental testing to provide closed-loop control for the position of pneumatic valves.[30] The calculation of heat release in real time has also been achieved in less than 0.02 CA at 1200 r/min on an FPGA, which can be used for HCCI combustion control.[31] An FPGA controller has been used to control the amount of injected fuel to prevent an overshoot of indicated mean effective pressure (IMEP) resulting from unburned fuel from the previous cycle[32] and it is proposed that a real-time calculation of exhaust gas fraction would improve the accuracy of the transferred fuel mass and allow for a better prediction of the fuel transferred from one cycle to the next. An FPGA has been used to calculate the real-time combustion metrics, CA50 and IMEP, which are then used for closed-loop control.[33] A physical model would improve the results by removing feed-forward maps and allow for disturbance rejection. This is the focus of the second part of this article, where the detailed physical gas exchange model is ported to FPGA hardware allowing for real-time calculation of in-cylinder temperature, pressure and trapped mass.

The procedure for the development and validation of a real-time capable FPGA-based gas exchange model is described in this article. This procedure can be broken into three stages of model development as depicted in Figure 1. The first step is the selection of a validated model based on physical governing equations. These equations are then used to develop a 0D physical gas exchange model created in MATLAB Simulink, subsequently referred to as offline physical model which is used for offline calculation of the cylinder temperature, pressure and trapped mass. The offline physical model is compared to a standard commercial gas exchange model as a simple validation. The offline physical model is used both as a reference for the real-time FPGA-based model and in the development of the FPGA model. The third step is the hardware implementation and experimental validation of the FPGA model. The offline physical model must be adapted in this step for implementation on the FPGA hardware. The focus here will be on the development of a gas exchange model for use with internal combustion engines utilizing negative valve overlap (NVO) to provide internal uncooled EGR, although a similar procedure can be followed for other FPGA algorithms. Each of the three steps will be explained in detail in the following sections.

Governing physical equations

The gas exchange process using the mass and energy conservation laws is formulated in the offline physical model which is spatially lumped. This 0D approach indicates that the physical quantities are independent of location, making the process parameters dependent of time only. The change in crank angle φ is related to the time domain via $d\varphi = \omega dt$, where ω is the angular engine velocity.

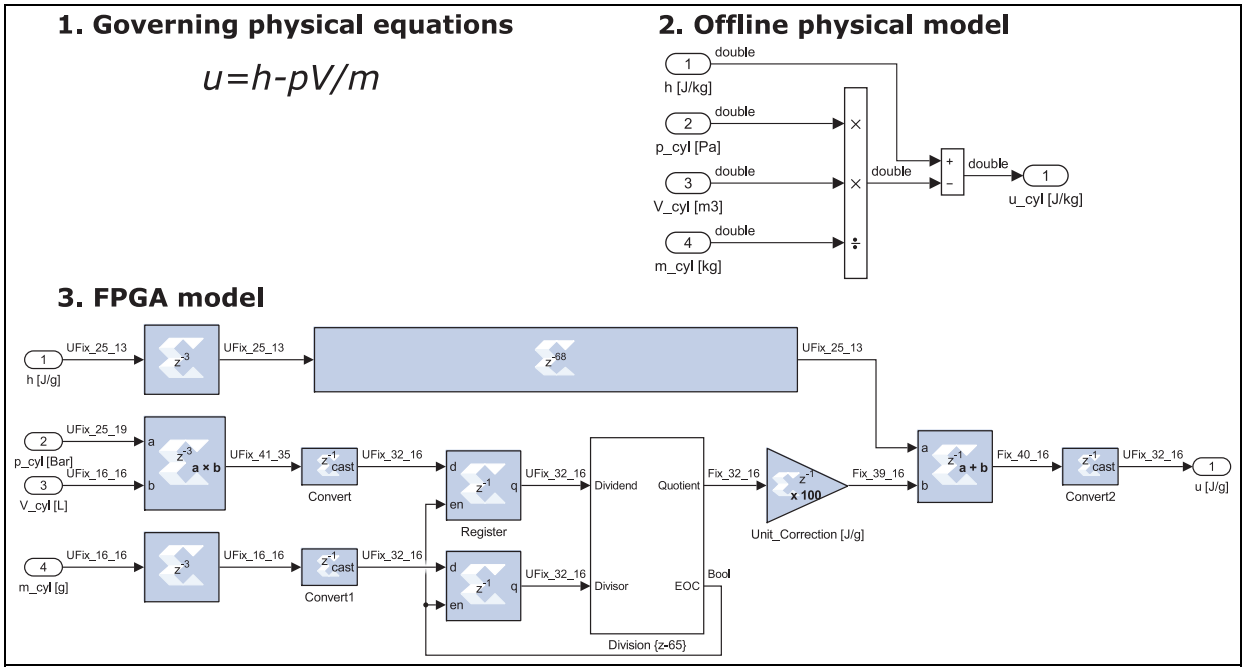

Figure 1. Example of the process to create an FPGA-based model from governing physical equations.

Energy conservation

The energy conservation neglecting kinetic energy and latent heat of fuel evaporation is

$$\frac{\mathrm{d}U}{\mathrm{d}\varphi} + \frac{\mathrm{d}Q_b}{\mathrm{d}\varphi} = \frac{\mathrm{d}Q_w}{\mathrm{d}\varphi} - p\frac{\mathrm{d}V}{\mathrm{d}\varphi} + \sum_i h_i \frac{\mathrm{d}m_i}{\mathrm{d}\varphi} \tag{1}$$

where $\mathrm{d}U/\mathrm{d}\varphi$ is the internal energy change, $\mathrm{d}Q_b/\mathrm{d}\varphi$ the fuel energy release, $\mathrm{d}Q_w/\mathrm{d}\varphi$ the wall heat transfer, $p\mathrm{d}V/\mathrm{d}\varphi$ the internal work and $h_i\mathrm{d}m_i/\mathrm{d}\varphi$ is the intake and exhaust enthalpy flows. Rewriting equation (1) to obtain an expression for the temperature gradient $\mathrm{d}T/\mathrm{d}\varphi$ results in

$$\frac{\mathrm{d}T}{\mathrm{d}\varphi} = \frac{-\frac{\mathrm{d}Q_b}{\mathrm{d}\varphi} + \frac{\mathrm{d}Q_w}{\mathrm{d}\varphi} - p\frac{\mathrm{d}V}{\mathrm{d}\varphi} + \sum_i (h_i - u_i)\frac{\mathrm{d}m_i}{\mathrm{d}\varphi}}{mc_v} \tag{2}$$

Based upon the measured crank angle–resolved cylinder pressure $p(\varphi)$, the heat release can be determined. It is defined that, during heat release, the transferred mass over the valves is zero. Additional simplifications can be made by neglecting the blow-by mass flow, assuming ideal gas state and constant gas composition $\mathrm{d}R/\mathrm{d}\varphi = 0$ and using the relations $R = c_p - c_v$ and $\gamma = c_p/c_v$. Using the specific heat ratio $\gamma(\varphi)$, the actual cylinder volume $V(\varphi)$ and the cylinder pressure $p(\varphi)$, all as a function of crank angle, the heat release term $\mathrm{d}Q_b/\mathrm{d}\varphi$ in equation (2) is modeled as

$$\frac{\mathrm{d}Q_b}{\mathrm{d}\varphi} = -\frac{1}{\gamma - 1}V\frac{\mathrm{d}p}{\mathrm{d}\varphi} - \frac{\gamma}{\gamma - 1}p\frac{\mathrm{d}V}{\mathrm{d}\varphi} + \frac{\mathrm{d}Q_w}{\mathrm{d}\varphi} \tag{3}$$

The heat transfer $\mathrm{d}Q_w/\mathrm{d}\varphi$ of the combustion engine cylinder charge to the walls is composed of convection and radiation.[34] To simplify, the radiation part is incorporated into the convective heat transfer coefficient α which is a good approximation for gasoline engines.[35] The wall heat transfer can be expressed as

$$\frac{\mathrm{d}Q_w}{\mathrm{d}\varphi} = \alpha(\varphi)A(\varphi)(T_w - T_{gas}(\varphi)) \tag{4}$$

To calculate the heat transfer, both the spatially averaged gas temperature in the cylinder $T_{gas}(\varphi)$ and the wall temperature T_w are required. The wall temperature is assumed constant ($T_w = 465\,\mathrm{K}$) over an entire cycle with a dependency on engine load and speed, and the charge temperature can be obtained from the equation of state 1.

To calculate wall heat transfer coefficient, $\alpha(\varphi)$, three commonly used correlations are Woschni,[36] Chang et al.[37] and Hohenberg.[38] For HCCI combustion, the Hohenberg correlation is recommended[39] and is

$$\alpha(\varphi) = 130V^{-0.06}p^{0.8}T^{-0.4}(\nu_{pis} + 1.4)^{0.8} \tag{5}$$

The piston speed ν_{pis} in equation (5) is calculated as a function of crank angle $\nu_{pis}(\varphi)$ in the model.

The internal energy u of the burned gas can be obtained from multiple modeling approaches.[40] A simplified approach where the internal energy is dependent on the gas temperature and air–fuel ratio is described in Justi.[41] This approach was then extended by Zacharias[42] to also consider the pressure dependency. However, both approaches are only valid for the Diesel process and an air–fuel ratio of $\lambda \geqslant 1$ and where the composition of the gas is assumed constant.

The combustion chamber can also be treated as a mixture of individual species for which each of the

species is considered an ideal gas.[43] The model is then based on polynomial curve fits to the thermodynamic data for each species in the mixture. The specific heat $c_{p,i}$ is approximated for each species i at temperature T as

$$\frac{c_{p,i}}{R} = a_{i,1} + a_{i,2}T + a_{i,3}T^2 + a_{i,4}T^3 + a_{i,5}T^4 \quad (6)$$

where the coefficients $a_{i,j}$ can be obtained from the tables. The enthalpy h of the species i is then given by

$$\frac{h_i}{R} = a_{i,1} + \frac{a_{i,2}}{2}T + \frac{a_{i,3}}{3}T^2 + \frac{a_{i,4}}{4}T^3 + \frac{a_{i,5}}{5}T^4 + \frac{a_{i,6}}{T} \quad (7)$$

The specific internal energy u of the species i can now be obtained by

$$u_i = h_i - RT \quad (8)$$

Using the species internal energies and their mass fractions χ, the internal energy of the mixture is

$$u_{mix} = \sum_i \chi_i \cdot u_i \quad (9)$$

which, as opposed to the previously mentioned modeling approaches, can be applied for any C/H ratio and a wider range of gases.

Mass conservation

The gas exchange process of the combustion chamber requires modeling of the intake and exhaust mass flows. The in-cylinder mass and composition at intake valve closing (IVC) can be determined using the mass flows and a mass balance. The theoretical (isentropic) one-dimensional (1D) stationary flow through a channel is defined as[44]

$$\frac{\mathrm{d}m_{th}}{\mathrm{d}\varphi} = A_s\rho_s\sqrt{\frac{2\gamma}{\gamma-1}RT_0\left[1-\left(\frac{p_1}{p_0}\right)^{\frac{\gamma-1}{\gamma}}\right]} \quad (10)$$

where ρ_s and A_s are the isentropic density and flow area and p_0 and p_1 are the pressure values before and after valve, respectively. Since the compression in a combustion engine is not isentropic and throttling losses occur, this equation must be tuned. To tune the model, an experimental flow measurement is required to measure the thermodynamical effect of the throttle losses. These losses are quantified by the irreversible increase in entropy. To do this, the mass flow through the valve is normalized to the theoretical (isentropic) mass flow. This throttle loss is expressed as a discharge coefficient C_d, which is defined as the relation between the experimental and theoretical mass flow as

$$C_d = \frac{\frac{\mathrm{d}m_{exp}}{\mathrm{d}\varphi}}{\frac{\mathrm{d}m_{th}}{\mathrm{d}\varphi}} \quad (11)$$

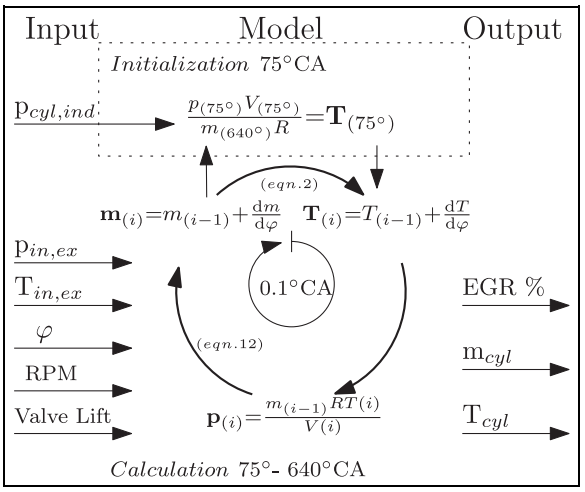

Figure 2. Schematic overview of the offline 0D physical gas exchange model created in Simulink.

The intake and exhaust mass flows are then calculated by substituting equation (11) into equation (10), where the indices 0 and 1 refer to before and after valve, respectively

$$\frac{\mathrm{d}m}{\mathrm{d}\varphi} = A_{th}C_d\rho_0\sqrt{2RT_0}\sqrt{\frac{\gamma}{\gamma-1}\left(\left(\frac{p_1}{p_0}\right)^{\frac{2}{\gamma}}-\left(\frac{p_1}{p_0}\right)^{\frac{\gamma+1}{\gamma}}\right)} \quad (12)$$

An injector model is used to estimate the injected fuel mass m_f as[32]

$$m_f = t_{inj}\alpha_f A\sqrt{2\rho_f\Delta p} \quad (13)$$

where t_{inj} is the the injection duration, Δp is the pressure difference between the fuel rail and the cylinder, ρ_f is the fuel density and A is the orifice area. The flow coefficient α_f is a function of t_{inj} to take the nonlinear opening and closing behavior of the injector into account. The injector model was calibrated on a test bench by performing multiple measurements.

Offline physical gas exchange model creation

To obtain crank angle–resolved information on the in-cylinder state during the gas exchange process, an offline physical 0D gas exchange model was created in MATLAB Simulink as shown schematically in Figure 2. The model input is a set of discrete test bench data: the intake, exhaust and indicated cylinder pressure, crank angle position and intake and exhaust temperature as well as the measured valve lift.

In this calculation loop, the calculated cylinder pressure is used instead of the indicated one. The motivation behind this is the unavoidable noise that is present in the indicated cylinder pressure, especially at valve closings. The mass flow calculation (equation (12)) is

extremely sensitive to pressure fluctuations and shows unrealistic results when using the measured cylinder pressure signal. Using a calculated cylinder pressure also helps compensate for sensor drift. During the combustion phase, –80 °CA to 75 °CA after top dead center (aTDC), the calculated pressure is set equal to the measured in-cylinder pressure, since no combustion model is currently incorporated.

The offline physical model is based on equations (2)–(13) with simplifications described in the previous section. A calculation loop applies the temperature gradient in equation (2) to calculate the current temperature, that is, $T_i = T_{i-1} + (\mathrm{d}T/\mathrm{d}\varphi)$, and other values of interest such as EGR% and cylinder mass m_{cyl} during one sample period. First, the indicated cylinder pressure is referenced using a thermodynamic zero-point correction to the intake manifold pressure to determine the absolute cylinder pressure and to initialize the model. Initialization takes place only once every cycle during the expansion phase before exhaust valve opening (EVO), and the in-cylinder temperature is calculated using the ideal gas law.

After initialization, the cylinder pressure is calculated from the cylinder temperature using the ideal gas law. This calculated cylinder pressure is combined with the measured manifold pressures to calculate cylinder mass using equation (12). This cylinder mass is then used in equation (2) to calculate the temperature gradient and subsequently the cylinder temperature. This calculation loop takes place during the gas exchange from before EVO at 75 °CA aTDC to after IVC at 640 °CA aTDC.

The calculated cylinder mass is used in the internal energy $u_i(\mathrm{d}m_i/\mathrm{d}\varphi)$ term in equation (2), and with the remaining four terms a temperature offset $\mathrm{d}T/\mathrm{d}\varphi$ is obtained to update the temperature of the next sample period. As a result, the calculated pressure, temperature and mass are delayed by one sample period. This delay is an important benefit of the model as it makes the model causal. This eliminates the need for a prediction in favor of rapid calculation.

The resolution of the model has an effect on the accuracy of the calculated parameters. In Figure 3, the cylinder mass has been modeled with four different resolutions. The model converges as the resolution increases from 5 °CA to 0.1 °CA which is the sample rate of the measured data. For this reason, a resolution of 0.1 °CA is used. For real-time implementation of a 0.1 °CA model, the computational speed of an FPGA is utilized in this work.

Model validation

An established commercial software, GT-Power®, which combines a 0D combustion calculation with a 1D gas exchange calculation was used as a reference model to validate the offline physical model.[7,10,24] The same test bench data are used as the input for both the offline physical and reference models for comparison and validation. The areas of interest for HCCI are the

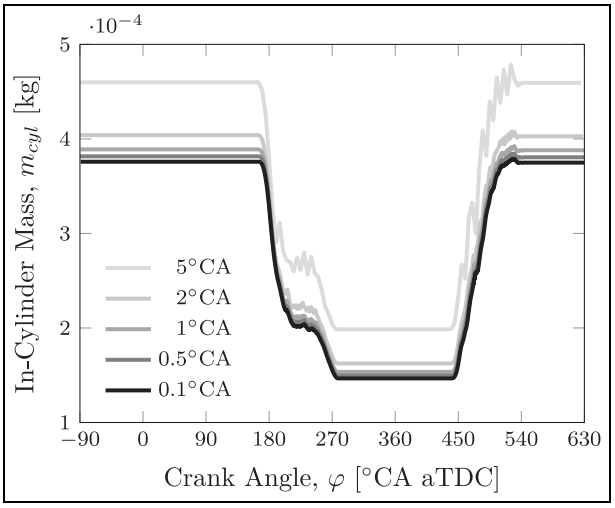

Figure 3. Effect of increasing model crank angle resolution on modeled cylinder mass.

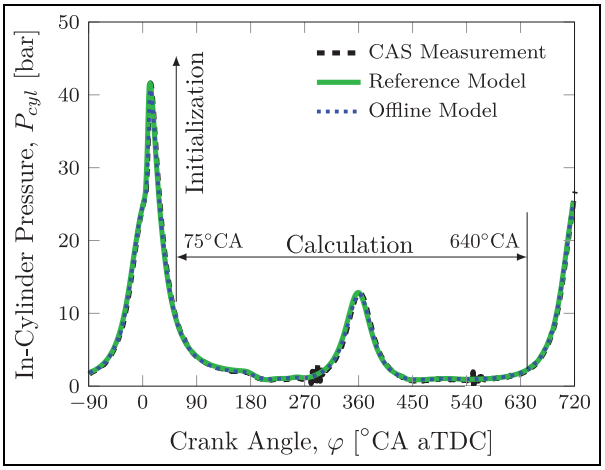

Figure 4. Validation of the modeled in-cylinder pressure with the reference model at 1500 r/min and 4.0 bar IMEP.

NVO recompression phase and valve events for the mass flow calculation. The first validation step was to compare the calculated in-cylinder pressure to the reference model and the measured pressure, as shown in Figure 4. The calculated in-cylinder pressure of the offline model matches the reference pressure trace quite well.

The 1D gas exchange process in the reference model incorporates gas dynamics, which include the spatial and temporal expansion of pressure waves in the intake and exhaust runner volumes, and the calculation of friction losses and wall heat transfer.[45] This inertia and spatial difference (sensor location) adds an additional phase shift effect to the pressure signals, therefore imposing a deviation in the mass flow calculation. To examine the impact of including the gas dynamics, the offline model was also simulated using intake and exhaust pressure traces that include the gas dynamics. These manifold pressure traces were extracted from the

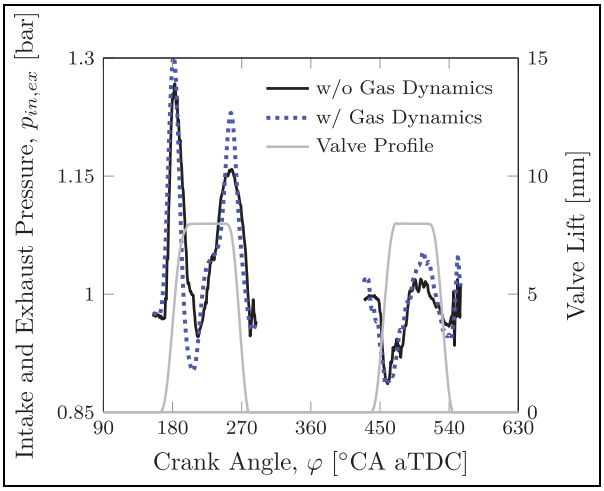

Figure 5. Comparison of the intake and exhaust pressure traces with and without incorporation of the gas dynamics at 1500 r/min and 4.0 bar IMEP.

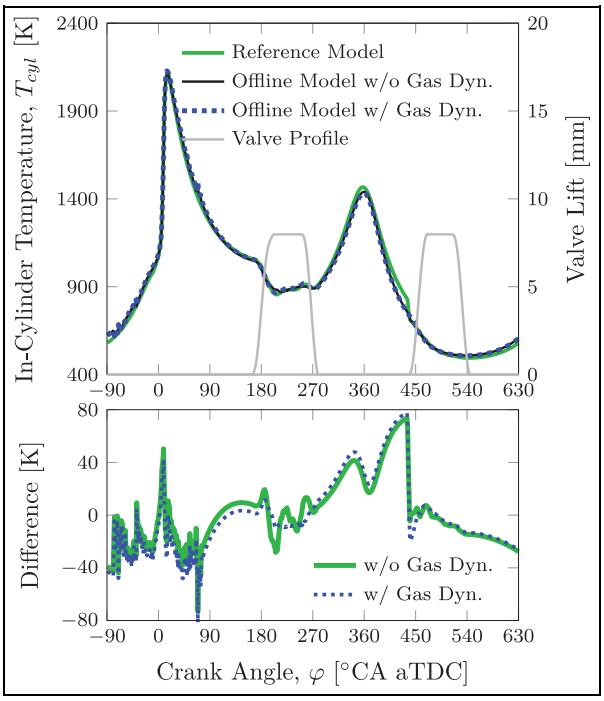

Figure 6. Validation of the modeled in-cylinder temperature with the reference model at 1500 r/min and 4.0 bar IMEP.

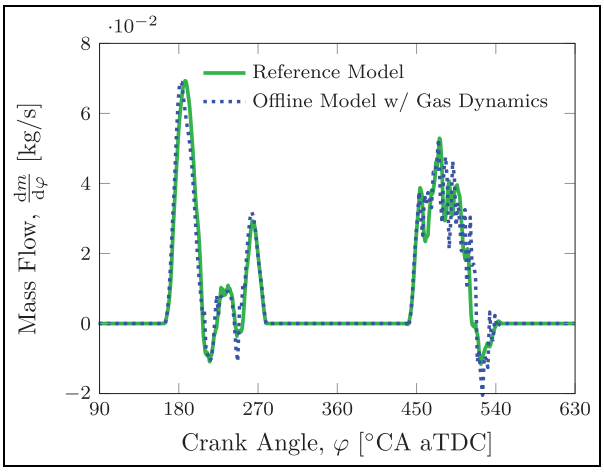

Figure 7. Validation of the modeled mass flow with the reference model at 1500 r/min and 4.0 bar IMEP.

reference model. In Figure 5, the raw measured manifold pressures without compensation for the gas dynamics and the manifold pressure traces corrected for gas dynamics have been shown. The gas dynamics appear to reduce the noise, as to be expected from the inertia of the exhaust and intake flow. Furthermore, the amplitude of the pressure fluctuations is increased in the pressure trace which considers gas dynamics.

The modeled in-cylinder temperature with and without consideration of gas dynamics, together with the reference temperature, is shown in Figure 6. The modeled temperature matches the reference temperature, especially during the valve events where a small difference of 25 K is seen. During NVO recompression, the temperature difference between the model and reference increases to 40 K. A larger deviation close to 80 K can be observed shortly before inlet valve opening (IVO) at the start of injection. The enthalpy of evaporation has not been modeled in the offline model, causing this small difference.

The mass flow rate with gas dynamics included is visualized in Figure 7, where the offline model approximates the reference mass flow rate very well. The pulses in the exhaust mass flow rate show the same amplitude and no phase delay. The same can be observed during the intake mass flow. Both models consider the backflow during valve events using the properties of the cylinder mixture at cylinder or manifold conditions depending on the flow direction.

Accumulation of the mass flow rates yields the cylinder mass, as shown in Figure 8. The offline model without gas dynamics deviates from the reference model during the exhaust phase and fails to simulate the rebreathing shortly before IVC. At these points, the deviation increases to 21.4 mg or 11.3% which can be seen in the model difference plot in Figure 8. However, a slight offset during the valve events is of less significance. On the other hand, the offline model with gas dynamics matches the reference model during these events. Despite the differences in the offline model due to the lack of gas dynamics, the cylinder mass is close, within 3 mg or 0.8%, when the valves are closed. As a result, the offline model is able to calculate the in-cylinder mass sufficiently well without the incorporation of gas dynamics.

An additional remark is that the masses at 90 °CA aTDC and 630 °CA aTDC are not identical. The cyclic and pressure fluctuations result in imbalanced exhaust and intake mass flows. Since the HCCI operation is unstable by nature, differences in mass flow and

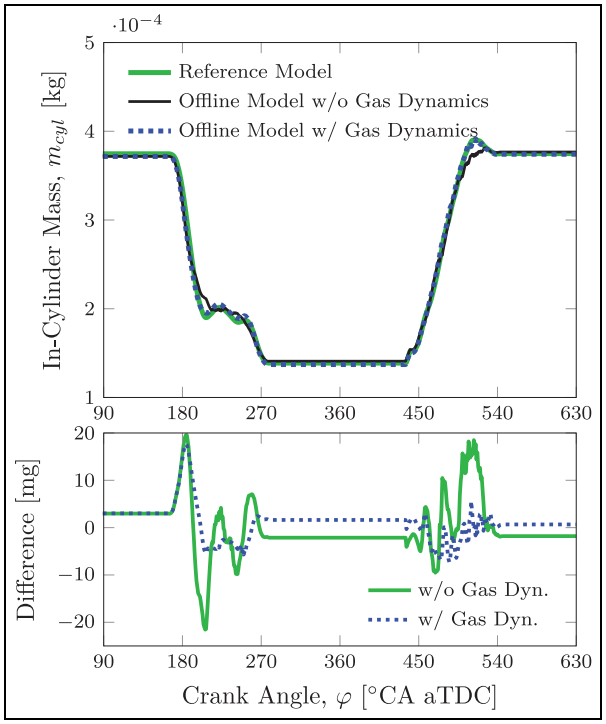

Figure 8. Validation of the modeled in-cylinder mass with the reference model at 1500 r/min and 4.0 bar IMEP.

trapped in-cylinder mass are expected. However, in the reference model each cycle is calculated by means of 200 iteration steps, until the steady state is reached. The output of one iteration step serves as the input for the following one. The offline physical model does converge due to its causal nature; however, it does not incorporate this iterative process which could result in minor differences in cylinder mass for large cyclic fluctuations. Despite these differences, the trapped in-cylinder mass matches the reference mass sufficiently well.

Conversion to FPGA

Converting equations (2)–(5) of the offline physical Simulink model to an FPGA-based model is the next step. To allow for the operation of the above Simulink-based gas exchange model on the Xilinx® FPGA hardware, the model must be adapted to use Xilinx System Generator (XSG) library blocks. These blocks are specifically designed to simplify the development of an FPGA-based model. The FPGA model creation consists of individually transferring each Simulink block from the offline physical model to its XSG equivalent while understanding the limitations of the FPGA hardware. Generally, the basic mathematical operations of addition, subtraction, multiplication and logical comparisons are resource efficient and can be easily implemented using the existing XSG blocks. However, many standard Simulink library blocks used in the offline physical model must be replaced with basic arithmetic for implementation on FPGA. In this work, the following mathematical operations are needed to be recreated to allow for the fixed point arithmetic used in the FPGA: division, windowed averaging, integration, moving average filtering and edge detection. An example of this transition from Simulink to XSG blocks is shown in Figure 1 and will be further explained in the following section.

FPGA hardware limitations

An FPGA consists of many gate arrays connected with reconfigurable routing fabric containing switch points or routing blocks between the gate arrays. The various logic blocks can be used for simple combination logic (lookup tables) or may be flip-flops which allow for sequential logic.[31,46] Also included on the FPGA board are random access memory (RAM) blocks distributed between the logic blocks which provide an efficient method for data storage.

A limitation of using gate arrays is that fixed point arithmetic must be used. This forces the model designer to consider the binary precision at every calculation (scaling of all variables) and also limits the mathematical arithmetic that is possible. The offline physical model, discussed above, allows for estimating the range of values that will result from each operation. It is also important to consider the value or specifically the binary position, of any two values before a mathematical operation to ensure that they are of similar size. This is to reduce calculation error due to an overflow or loss in precision due to truncation of the result. In the development of the gas exchange model, due to the large magnitude difference in SI units for pressure, volume and temperature, this problem occurs and scaling must be used. This however creates the additional step of checking the units after a calculation and possible unit correction before subsequent calculations. Figure 1 shows the signal sizes before and after each mathematical operation. To reduce the binary size of the signal the "cast" block is used to truncate extra bits. This reduces not only the precision of the number, but also the resources that are required on the FPGA. Correctly setting the binary size is important in allocating the correct amount of resources to extremely sensitive calculations while saving resources by reducing the bit size for calculations that do not require it.

Figure 1 is also a good example of the limitation of FPGA arithmetic. Here the division is performed using a binary division algorithm which takes 65 samples and consumes significant FPGA resources when compared to addition, subtraction or multiplication. It also requires registers before the calculation to hold the incoming values constant during the calculation period. Another limitation of the binary division algorithm used is that it requires a 32-bit signal with a binary point of 16, further strengthening the requirement to estimate the values which are divided when performing fixed point arithmetic.

Table 1. Included physical phenomenon in offline and FPGA models.

Physical process	Offline model	FPGA online model
Energy conservation, equation (2)	Included	Included
Hohenberg wall heat model, equation (5)	Included	Included
Orifice flow, equation (12)	Included	Included
Heat release during recompression	Included	Neglected
Gas dynamics	GT-Power corrected manifold pressure	Neglected
Injected fuel mass, equation (13)	Included	Neglected
Ratio of specific heats, γ	NASA polynomials	2nd-order polynomial simplification
Intake air properties	NASA polynomials	Assumed constant
Specific heat of cylinder gas	NASA polynomials	Temperature-dependent lookup table
Enthalpy of cylinder contents	NASA polynomials	Temperature-dependent lookup table

Porting the model to the FPGA must take into account the limited number of gate arrays and RAM blocks. This requires that the model is kept as simple as possible to conserve available resources. A trade-off between gate array and RAM usage is often considered to determine if a complex calculation requiring many gates should be simplified to a 1D lookup table that requires more RAM. Specifically, the calculation of the piston speed, ν, required in equation (5), contains trigonometric functions that are difficult and resource intensive to implement using standard fixed point arithmetic. This was an example where a lookup table was used to conserve gate array resources.

FPGA delay consideration

One major difference between a standard microprocessor-based model such as the offline physical model and the model ported to the FPGA is that on FPGA each calculation consumes a fixed amount of time. As many calculations are occurring in parallel on the FPGA, this can cause signals to become delayed and misaligned if the time for the signal to pass through each logic element is ignored. The amount of delay is dependent on the complexity of the calculation taking place, but at least one sample period (12.5 ns on the FPGA used in this study) occurs. This delay is shown in Figure 1 where the mass signal must be delayed by three samples to match the delay caused by the multiplication of pressure and volume. This ensures that both signals being divided are correctly synchronized in time.

The individual delays of each operation on the FPGA can then be summed to determine the total calculation time. For the entire gas exchange process on the FPGA, the calculation time is 282 samples or 3.5250 μs. Therefore, with the current FPGA model running at 0.1 °CA, an engine speed of up to 4728 r/min is possible. If higher engine speeds are desired, the calculations could be performed at a lower resolution. For example, calculating at 0.2 °CA would double the maximum engine speed. The impact from the reduction in resolution is small as shown in Figure 3.

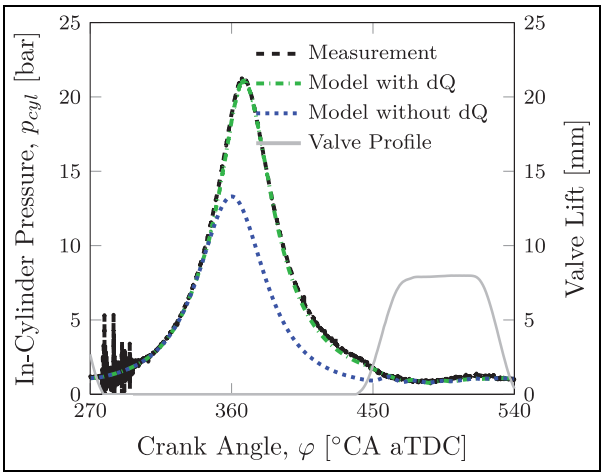

Figure 9. In-cylinder pressure during the NVO recompression phase. The offline physical model is able to accurately capture the heat release if combustion occurs and calculate the correct cylinder pressure.

Model physics reduction

To port the offline physical model to the FPGA capable model, simplification of a portion of the physics used in the offline model is used. The three main changes were neglecting the heat release from possible combustion in the NVO recompression phase, not considering gas dynamics and a simplification of the NASA polynomials for the gas properties. The model simplifications for FPGA implementation are summarized in Table 1.

Consideration of combustion reactions during the NVO recompression phase is an important effect to incorporate if there is a misfire in the previous cycle. The heat release during the NVO phase $\mathrm{d}Q_{NVO}/\mathrm{d}\varphi$ has been modeled according to equation (3). In Figure 9, the effect of including the heat release $\mathrm{d}Q_{NVO}/\mathrm{d}\varphi$ on the in-cylinder pressure is visualized.

As shown in Figure 9, the model without heat release fails to simulate the combustion, leading to a difference in peak pressure of 10 bar. However, the NVO combustion as shown in Figure 9 is an extreme scenario which occurred approximately once every 100 cycles at a very unstable operating point. The choice of neglecting the

combustion during intermediate compression was made to simplify the model for FPGA implementation. Since combustion during recompression is not desired and only occurs sporadically under extreme operating conditions, the simplification is acceptable.

As discussed in the offline model section, the inclusion of gas dynamics allows for a better match between the offline physical and reference models. However, the cylinder temperature and mass are very close between the models and the inclusion of gas dynamics adds complexity to the FPGA model. Therefore, currently the gas dynamics are excluded from the FPGA model for simplicity and resource conservation.

The offline physical model calculates the gas properties using NASA polynomials using equation (6). To conserve resources and simplify the FPGA model, the gas properties were simplified to either constant values or a temperature-dependent lookup table. To determine if a lookup table was necessary rather than a constant value, the values calculated in the physical model were examined. Values that have little variation over the range that they are used were set as constants. For example, the intake and exhaust manifold temperatures do not vary significantly over a single valve event and therefore it was sufficient to leave them as constants. As the temperature in the intake manifold remains constant so does the density, gas constant and enthalpy of the charge entering the cylinder.

This simplification, however, cannot be applied to the cylinder contents as the cylinder temperature changes over the exhaust event which changes the properties of the gas leaving the cylinder. Therefore, it was necessary to calculate the cylinder density, gas constant and enthalpy using temperature-dependent lookup tables.

The specific heat ratio, γ, is one gas property that has a significant impact on the calculated cylinder temperature. To get an acceptable value, it is necessary to use the following second-order polynomial[47]

$$\gamma = 1.338 - 6.0 * 10^{-5} T + 1 * 10^{-8} T^2 \quad (14)$$

where T is the calculated cylinder temperature. Using this equation allowed for a good approximation of the specific heat ratio without the need for a detailed lookup table and is arithmetically simpler to implement than the fourth-order NASA polynomials. Equation (14) provides a good balance of the required accuracy and FPGA resource conservation.

FPGA model error sources

The porting of the offline physical model to an FPGA capable model involves two main sources of error. These errors result from switching to fixed point arithmetic over using floating point operations and the error caused by simplifying the physics in the model. Figure 10(a) shows the calculated constant volume specific heat capacity c_v at various temperatures. This figure

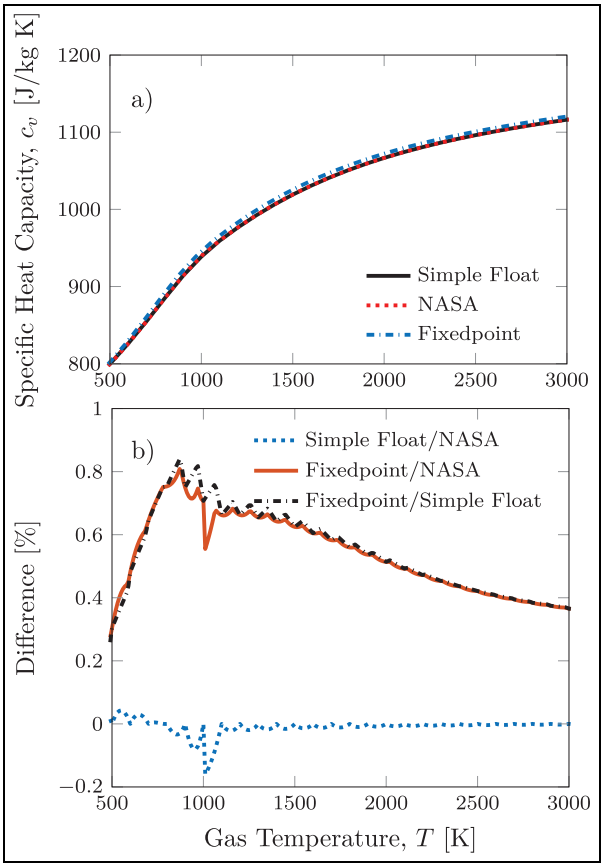

Figure 10. Difference in constant volume specific heat capacity due to transition to FPGA capable model.

shows the calculation using NASA polynomials and floating point arithmetic, simplified lookup table results using floating point arithmetic and finally the fixed point lookup table results. Here very little variation can be seen between the three calculation methods.

Figure 10(b) shows the difference between the three calculations. Here the simple floating point model matches the NASA polynomials; however, the transition to fixed point arithmetic causes an increase in the difference between calculations. Here the difference between the FPGA model using the fixed point arithmetic and the NASA values used in the offline model is less than 1%. This value is acceptable as the model output changes very little for the additional resource cost of increasing binary size.

Offline FPGA simulation

For offline simulation of the FPGA model, these small sections of the existing offline physical model were individually converted over to XSG blocks. Then using the offline physical model as the input for offline simulation of the FPGA model, small sections of the FPGA model can be optimized. The output of the FPGA model was then compared to the offline physical model results and adjustments to binary precision were made as necessary. Thus, having a good offline physical

model is essential to generate values that cannot be measured experimentally.

The problem with running an offline FPGA simulation is the simulation time of 720 °CA taking over 21 h compared to under 5 s for the same cycle using the offline physical model when the simulations are run on an Intel Core i7-6700K-based PC. For comparison, in the case of online FPGA the engine cycle can be run in 25.4 ms. This means that simulations must be carefully planned and results saved at intermediate calculations to troubleshoot after completion. The slow simulation is a consequence that each FPGA time step is simulated which is 12.5 ns or 887 steps per 0.1 °CA at an engine speed of 1500 r/min used in this study.

After the small sections are individually tested in offline FPGA simulations, they can be combined to build up the complete operation and then the complete model. As previously discussed, the parallel processing of the FPGA presets a timing issue. When combining the small sections, it is essential to ensure the correct accumulated delay of each model section. This is important so that the values are updated at the same time and signals of different delay are not combined in future operations. After combining the smaller sections, another simulation is run and the results are compared to the offline physical model to check for errors caused by incompatible binary precision and timing problems.

Experimental setup

A single cylinder research engine (SCRE) outfitted with a fully variable electromagnetic valve train (EMVT) is used to validate the online FPGA gas exchange model. The EMVT is controlled using the FPGA board which is part of the engine control unit (ECU). The flexibility of the valve timing allows for engine operation with combustion chamber EGR through NVO. This allows for a wide operating range of HCCI combustion timings. The cylinder head used for the experiments is designed for optical investigations but no optical measurements were made. However, the sealing between the head and cylinder sleeve causes higher blow-by than a metal engine. The fuel injector is a piezoelectric outward opening hollow cone injector that is controlled using the FPGA. The fuel used for all testing in this work is conventional European Research Octane Number (RON) 96 gasoline containing 10% ethanol. Engine geometry and testing conditions are listed in Table 2.

The four main inputs to the gas exchange model are cylinder, intake and exhaust manifold pressures and crank position. The in-cylinder pressure is measured using a Kistler A6061B piezoelectric pressure transducer. The intake and exhaust manifold pressures are measured using Kistler 4045-A5 piezoresistive pressure transducers. Kistler charge amplifiers are used to output the measured pressure as a voltage. The positions of the electromagnetic valves are measured using FEV conductive lift measurement sensors, while the position of the crank is measured using a Hall effect encoder.

Table 2. Single cylinder research engine parameters.

Parameter	Value
Displacement volume	0.499 L
Stroke	90 mm
Bore	84 mm
Compression ratio	12:1
No. of valves (In/Ex)	2/2
Valve train	EMVT
Max. valve lift (In/Ex)	8 mm/8 mm
Valve angle (In/Ex)	22.5°/22.5°
Valve diameter (In/Ex)	32 mm/26 mm
Intake air pressure	1013 mbar
Exhaust pressure	1013 mbar
Oil and coolant temperature	90 °C
Engine speed	1500 r/min
Fuel rail pressure	100 bar
Intake temperature	50 °C

EMVT: electromagnetic valve train.

Table 3. Rapid prototyping ECU specifications.

	Parameter	Specification
Processor	dSPACE® 1401	IBM PPC-750GL
	Speed	900 MHz
	Memory	16 MB main memory
I/O board	dSPACE 1513	
	Analog input	24 parallel channels
	Resolution	16 bit
	Sampling frequency	1 Msps
	Analog input	32 multiplexed channels
	Resolution	16 bit
	Sampling frequency	200 Ksps
	Analog output	12 channels
	Digital input	40 channels
	Digital output	40 channels
FPGA	dSPACE 1514	Xilinx Kintex-7
	Flip-flops	407,600
	Lookup table	203,800
	Memory lookup table	64,000
	Block RAM	445
	Digital signal processing	840
	I/O	478

FPGA: field programmable gate array.

An FEV combustion analysis system (CAS) is used to record cylinder pressure at a 0.1° resolution for use in the offline detailed model. The pressure signals are simultaneously input to the FPGA board contained in the prototyping ECU. Details of the MicroAutoBox II (MABX) prototyping ECU are provided in Table 3.

Resource utilization

As the hardware resources are limited for FPGA implementation, it is important to consider the resource utilization for model development. These resources are broken into six main categories as presented in Table 3.

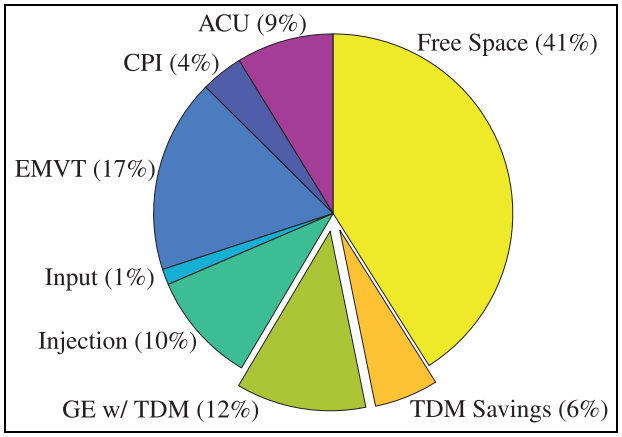

Figure 11. Lookup table resource utilization from the current model sub-systems.

The FPGA lookup tables' resource usage from each of the main model sub-systems is visualized in Figure 11. This figure is also useful in analyzing which model subsystem is utilizing resources. Here it can be seen that the gas exchange model is not using the most resources, but the EMVT valve and injection control utilize a significant portion of the resources. In addition, there still remain free resources that can be used for future controllers.

The resource savings made available using time division multiplexing (TDM) on the mass flow can be seen as a large percentage in Figure 11 of the total resources used in the gas exchange model. The similarity of calculations between the intake and exhaust mass flows and the high calculation speed of the FPGA are combined to conserve resources. This is accomplished by alternating the input values between intake and exhaust every sample (12.5 ns) and then passing that signal through the FPGA logic blocks to complete the mass flow calculation, then separating the two signals after the calculation as shown in Figure 12. This is only possible as the mass flow calculation on FPGA occurs much faster than the intake pressure changes at 0.1 °CA. This allows the same hardware on the FPGA to be used for the calculation of the both mass flows.

Another benefit of utilizing FPGA hardware over standard microprocessor-based engine controllers is that the hardware requirements do not vary depending on the engine speed. Each mathematical operation on the FPGA hardware requires a fixed amount of time and utilizes specific resources. When the model is flashed to the FPGA, the hardware resources are consumed and do not vary.

Results of the online FPGA model

After verifying that the offline FPGA simulation results were within 5% of the offline physical model, the FPGA model was compiled and flashed to the FPGA hardware for online testing and further tuning. The CAS system was set to output a timing pulse at the start of recording which was then recorded on both the MABX and CAS systems. This timing pulse was used to align the online FPGA model with the identical CAS cycle. Having the CAS data cycle synchronized with the FPGA data ensures that the offline physical model calculates the same cycle to have results that capture the cyclic variability present in HCCI combustion.

The FPGA results presented in this section were calculated on the FPGA board and recorded on the processor side of the ECU. The extraction of values to the processor side was limited to a sampling rate of 0.5 ms to prevent overruns. However, it should be noted that the FPGA is still calculating at 12.5 ns, and this fast sampling rate can be used for FPGA-based controllers.

The calculation of cylinder pressure using the online FPGA model is compared to the measured and offline physical model–calculated pressures shown in Figure 13. The cylinder pressure matches well over the entire engine cycle. During the NVO recompression, there is a slight difference between the cylinder pressures calculated using the models and the measured pressure. This pressure difference is attributed to blow-by due to poor sealing between the optical cylinder head and the piston sleeve. This pressure loss is not included in the model and can be seen by the over-prediction of cylinder pressure during recompression. This error would be significantly lower for a metal engine and is not seen as a deficiency with the model.

The calculation of the temperature gradient presented in equation (2) is used for the calculation of the cylinder temperature from the previous time step. Therefore, it is important that the online FPGA model matches the offline physical model. Figure 14 shows that both models match with only a very slight offset during NVO recompression. This offset is attributed to simplifications in the wall heat loss calculation in the FPGA model.

As the temperature gradient closely matches the physical model, this leads to an accurate cylinder temperature calculation as shown in Figure 15. During the gas exchange process, both models are very close. However, the temperatures calculated during the combustion phase show some difference. As explained above, during the combustion phase, the cylinder

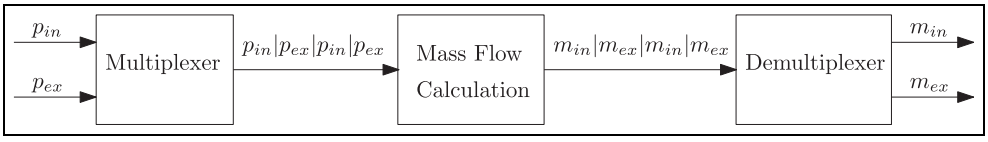

Figure 12. Process of time division multiplexing.

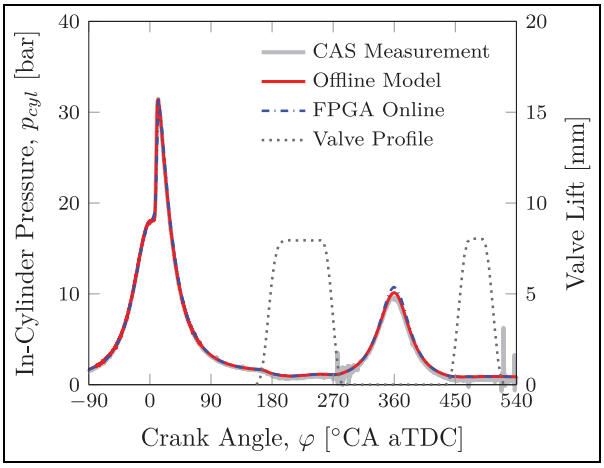

Figure 13. Comparison of the measured in-cylinder pressure with the values calculated using the offline physical model and the online FPGA model.

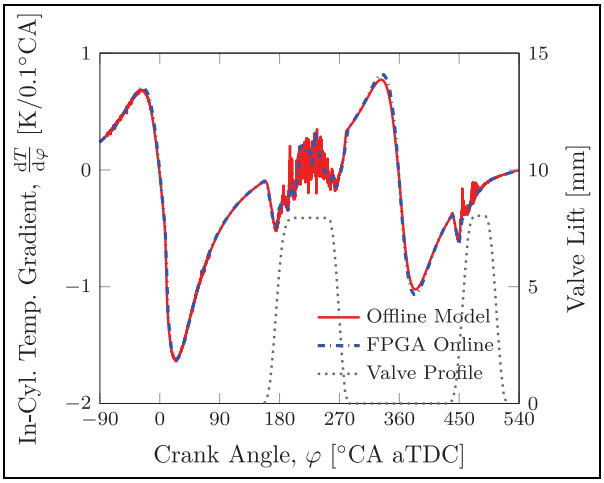

Figure 14. Comparison of temperature gradient calculated with the offline physical model and the online FPGA model.

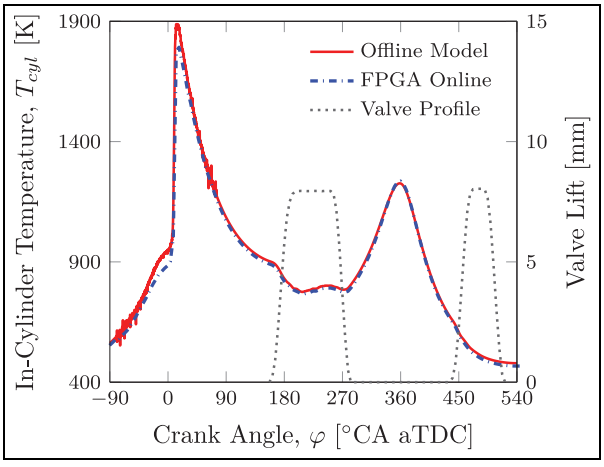

Figure 15. Comparison of temperature calculated with the offline physical model and the online FPGA model.

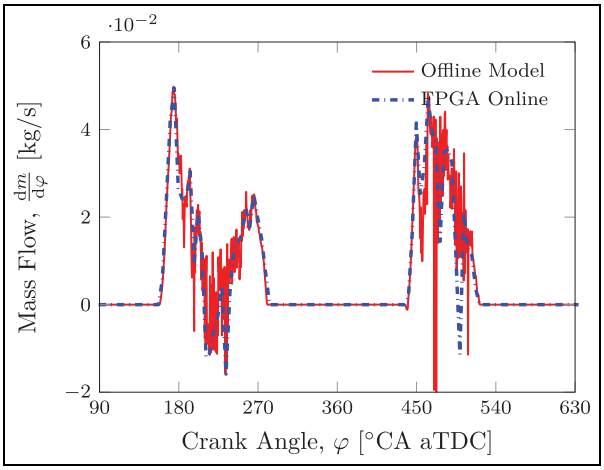

Figure 16. Comparison of cylinder mass flow calculated with the offline physical model and the online FPGA model.

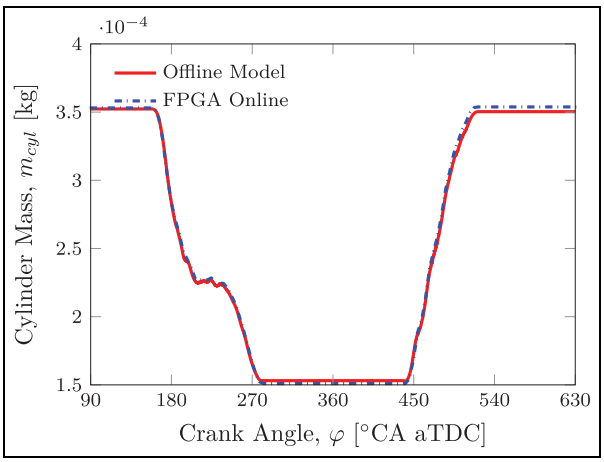

Figure 17. Comparison of trapped cylinder mass calculated with the offline physical model and the online FPGA model.

temperature is calculated using the ideal gas law and not the first law of thermodynamics as it is during the gas exchange process. Therefore, the FPGA model only needs to calculate the temperature during combustion to use as an initialization value. The causal nature of the model means that the initialization value does not need to be exact and this opportunity was used to conserve FPGA resources.

Figure 16 shows the air mass flow rate calculated on both models using equation (12). The flow rates are very similar with the main difference being that the FPGA model appears smoother due to the limited sampling rate of the ECU processor as described above. As the mass flows of the models are very similar, both models calculate a similar cylinder mass as shown in Figure 17.

Model flexibility

A physics-based model can handle a wide range of operating conditions compared to a linearized model.

Table 4. Difference in calculated fresh air ratio between the FPGA and offline physical models for variation in engine speed, NVO and boost pressure.

RPM (1/min)	NVO (°CA)	Boost (mbar)	IMEP (bar)	Mean error (%)	Std σ error (%)	Max error (%)
1000	170	1013	2.94	−0.19	0.53	2.71
1250	170	1013	2.92	−0.22	0.59	3.13
1500	170	1013	2.64	−0.23	1.41	3.73
1700	170	1013	2.57	−0.34	1.43	2.31
1500	*197*	1013	2.04	−0.28	1.34	3.54
1500	*170*	1013	2.64	−0.23	1.41	3.73
1500	*150*	1013	2.77	−0.42	1.70	3.42
1500	*130*	1013	3.26	−0.35	1.27	2.30
1500	164	*967*	2.19	−0.20	1.24	4.05
1500	164	*1110*	2.63	−0.081	1.02	3.50
1500	164	*1200*	2.63	+0.16	1.22	4.40
1500	164	*1300*	2.79	−0.004	1.24	3.50

RPM: revolutions per minute; IMEP: indicated mean effective pressure.Italicized values represent the manipulated variables for each sweep.

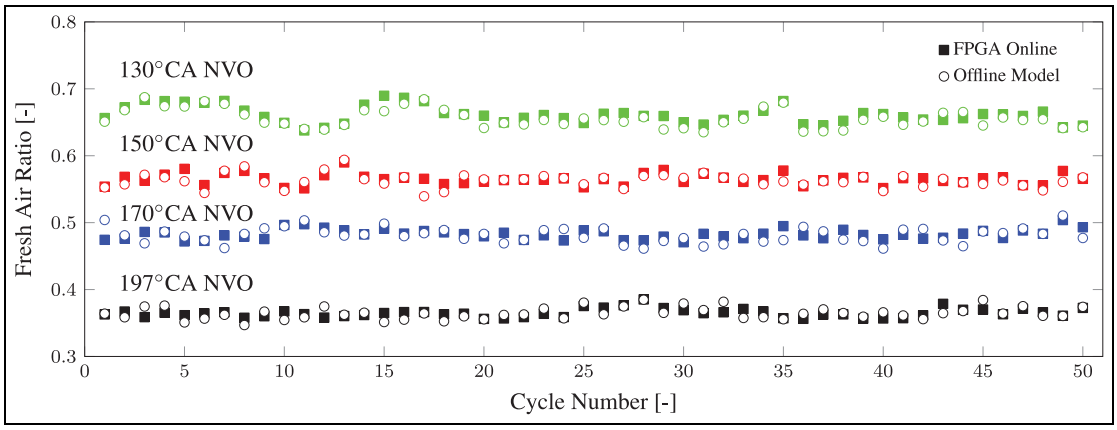

Figure 18. Fresh air ratio comparison for various NVO durations. Note that with increasing fresh air ratio the IMEP increases.

This means that variations in engine speed, boost pressure and NVO can be handled by the model without the need to linearize the model at many operating points, that is, engine mapping. This makes the physics-based model capable of handling many operating points and also allows for disturbances to be accurately included in the calculation.

To test the models' ability to handle various operating points, three sweeps were performed: boost pressure, NVO duration and engine speed. These changes represent control variables for HCCI combustion timing that could be encountered in practical engine operation. Boost pressure can be used to increase the operation range, however, not for cycle-by-cycle control.[20] Since the SCRE is equipped with a fully variable EMVT, an NVO sweep can be achieved in various ways. In this study, the NVO was kept symmetric around the gas exchange top dead center (TDC). The EVO and IVC were fixed during this sweep, while exhaust valve closing (EVC) and IVO were symmetrically varied, starting at the largest NVO. The third sweep was a variation of engine speed. Autoignition requires time for the chemical reactions to occur and increased engine speed reduces the time the cylinder contents spend at increased temperature and pressure. Variations in engine speed are also expected in practical implementations of HCCI combustion so it is important that the model should be able to handle this change in boundary conditions. The chosen operating points of these three sweeps are presented in Table 4.

To compare the offline and FPGA models at the various operating points, the fresh air ratio was derived from the continuous mass calculation. This is the ratio of the fresh air entering the combustion chamber during the intake event to the total cylinder mass defined as

$$Fresh\ air\ ratio = \frac{m_{fresh\ air}}{m_{total}} = \frac{m_{IVC} - m_{IVO}}{m_{IVC}} \tag{15}$$

The fresh air ratio for a variety of NVO durations for 50 cycles is shown in Figure 18. Here the FPGA model is able to follow the trend of the offline physical model capturing the cyclic variance in the fresh air ratio which has an effect on HCCI combustion timing. As both models are physics based, they both capture the change in NVO duration.

To obtain a measure for the FPGA model accuracy, a relative error is defined as the percentual difference between the FPGA and offline models of the fresh air

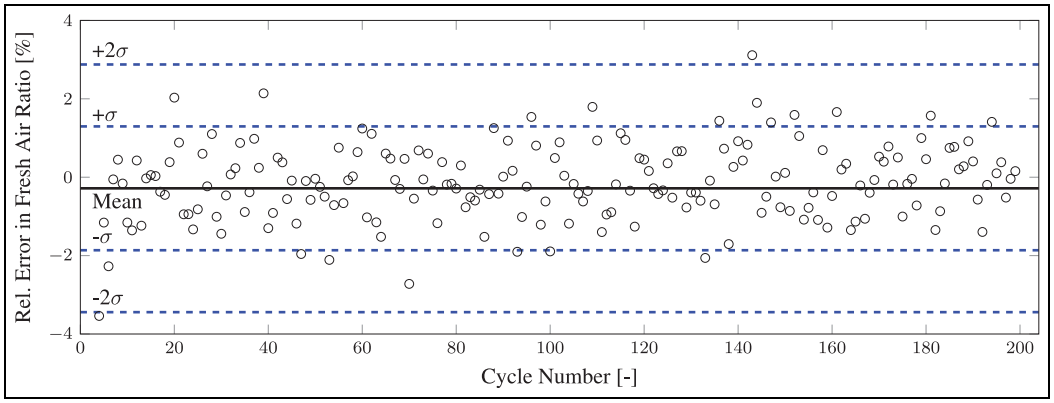

Figure 19. Percent difference in fresh air ratio between the models for NVO duration of 170 °CA.

ratio. Figure 19 shows the relative error for each cycle as well as the mean error and standard deviation, σ, over the 200 cycles for a specific measurement point. As can be concluded from the figure, the relative error for all 200 cycles remains below 4% in this measurement point. These values along with the maximum error over all 200 cycles for all 12 measurements are listed in Table 4. As can be seen, the mean error fluctuates around zero for all measurements showing that there is not a bias in the model to over- or under-predict the fresh air ratio when compared to the offline physical model. The standard deviation σ, which gives information on the amount of variation of the individual points in the entire measurement, reaches a maximum of 1.70% during all three sweeps. This indicates that the relative errors are close to the mean, and that the FPGA model works well over a variety of operating points. A maximum error of 4.40% over all 12 measurements indicates that the FPGA model achieves a good match to the offline physical model.

Conclusion and future work

The FPGA gas exchange model presented in this article is real time capable and has been experimentally validated to the physically based 0D offline Simulink and reference GT-Power models. This validation has not only shown that the FPGA model matches the offline physical model at the desired operating point, but also for a wide range of operating points. Since the model is physics based, a range of operating conditions can be accurately simulated without the need for parameterizing lookup tables that have been used in previous real-time gas exchange models. The physical basis of the model allows for more detailed physics to be added where needed to improve the accuracy of the model output. The process of converting governing physical equations to a real-time capable FPGA model has been demonstrated and can be applied to a variety of systems where rapid calculations are required.

The benefit of using FPGA hardware for implementation of the gas exchange process is that the cylinder state is calculated after only 0.1 °CA. This offers the potential to implement new HCCI control strategies that require current cylinder state. These control strategies rely on real-time cylinder mass, temperature and residual gas fraction to implement in-cycle feedback controllers to extend the HCCI operation range and increase combustion stability. In-cycle water injection using the current cylinder state to control combustion timing is one application where the presented FPGA model can be used and is the subject of our future work.

Declaration of conflicting interests

The author(s) declared no potential conflicts of interest with respect to the research, authorship and/or publication of this article.

Funding

The author(s) disclosed receipt of the following financial support for the research, authorship, and/or publication of this article: This work was performed in preparation of the research group 2401, funded by Deutsche Forschungsgemeinschaft (DFG) and with the Natural Sciences Research Council of Canada under Grant No. 2016-04646. Partial funding from Future Energy Systems at the University of Alberta is also gratefully acknowledged.

ORCID iDs

David Gordon https://orcid.org/0000-0002-7999-8234
Christian Wouters https://orcid.org/0000-0002-2562-3146
Maximilian Wick https://orcid.org/0000-0001-5033-930X
Jakob Andert https://orcid.org/0000-0002-6754-1907

References

1. Breitbach H, Waltner A, Landenfeld T and Schwarz C. Lean-burn stratified combustion at gasoline engines. *MTZ Worldwide* 2013; 74(5): 10–16.
2. Langen P, Melcher T, Missy S, Schwarz C and Schünemann E. Neue BMW Sechs- und Vierzylinder-Ottomotoren mit High Precision Injection und Schichtbrennverfahren. In: *28th Internationales Wiener*

Motorensymposium, Vienna, 26–27 April 2007. Austrian Society of Automotive Engineers.
3. Waltner A, Lückert P, Schaupp U, Rau E, Kemmler R and Weller R. Die Zukunftstechnologie des Ottomotors: strahlgeführte Direkteinspritzung mit Piezo-Injektor. In: *27th Internationales Wiener Motorensymposium*, Vienna, 26–27 April 2006, pp.24–43. Austrian Society of Automotive Engineers.
4. Zhao H. *HCCI and CAI engines for the automotive industry*. Boca Raton, FL: Woodhead Publishing in Mechanical Engineering, 2007.
5. Guibert P, Morin C and Mokhtari S. Verbrennungssteuerung durch Selbstzündung. *MTZ—Motortechnische Zeitschrift* 2004; 65(2): 122–130.
6. Stan C and Guibert P. Verbrennungssteuerung durch Selbstzündung. *MTZ—Motortechnische Zeitschrift* 2004; 65(1): 56–62.
7. Brassat A. *Betriebsstrategien der kontrollierten Selbstzündung am aufgeladenen direkteinspritzenden Ottomotor*. PhD Dissertation, RWTH Aachen University, Aachen, 2013.
8. Bücker C. *Betriebsstrategien zur kontrollierten Selbstzündung in Ottomotoren*. PhD Dissertation, RWTH Aachen University, Aachen, 2008.
9. Kulzer A, Fischer W, Karrelmeyer R, Sauer C, Wintrich T and Benninger K. Kontrollierte Selbstzündung beim Ottomotor CO2 Einsparpotenziale. *MTZ—Motortechnische Zeitschrift* 2009; 70(1): 50–57.
10. Seebach D. *Untersuchung der kontrollierten Selbstzündung an einem direkteinspritzenden Ottomotor und Modellierung des transienten Verhaltens*. PhD Dissertation, RWTH Aachen University, Aachen, 2010.
11. Ebrahimi K. *Model based control of combustion timing and load in HCCI engines*. PhD Dissertation, University of Alberta, Edmonton, AB, Canada, 2016.
12. Maurya RK and Agarwal AK. Experimental study of combustion and emission characteristics of ethanol fuelled port injected homogeneous charge compression ignition (HCCI) combustion engine. *Appl Energ* 2011; 88(4): 1169–1180.
13. Haraldsson G, Tunestl P, Johansson B and Hyvnen J. HCCI combustion phasing with closed-loop combustion control using variable compression ratio in a multi cylinder engine. SAE technical paper 2003-01-1830, 2003.
14. Manofsky L, Vavra J, Assanis D and Babajimopoulos A. Bridging the gap between HCCI and SI: spark-assisted compression ignition. SAE technical paper 2011-01-1179, 2011.
15. Slepicka CE. *Iterative learning control for fuel robust HCCI*. MSc Thesis, University of Alberta, Edmonton, AB, Canada, 2016.
16. Kirchen P, Shahbakhti M and Koch CR. A skeletal kinetic mechanism for PRF combustion in HCCI engines. *Combust Sci Technol* 2007; 179(6): 1059–1083.
17. Kokjohn SL, Hanson RM, Splitter DA and Reitz RD. Experiments and modeling of dual-fuel HCCI and PCCI combustion using in-cylinder fuel blending. *SAE Int J Engines* 2010; 2: 24–39.
18. Ghazimirsaied A and Koch CR. Controlling cyclic combustion timing variations using a symbol-statistics predictive approach in an HCCI engine. *Appl Energ* 2012; 92: 133–146.
19. Saxena S and Bedoya ID. Fundamental phenomena affecting low temperature combustion and HCCI engines, high load limits and strategies for extending these limits. *Prog Energ Combust* 2013; 39(5): 457–488.
20. Lehrheuer B, Morcinkowski B, Pischinger S and Nijs M. Low temperature gasoline combustion—potential, challenges, process modeling and control. In: King R (ed.) *Active flow and combustion control 2014* (Notes on numerical fluid mechanics and multidisciplinary design), vol. 127. Cham: Springer, 2015, pp.163–179.
21. Andert J. *Modellbasierte Echtzeitoptimierung der ottomotorischen Selbstzündung*. PhD Dissertation, RWTH Aachen University, Aachen, 2012.
22. Hellstrom E, Larimore J, Jade S, Stefanopoulou AG and Jiang L. Reducing cyclic variability while regulating combustion phasing in a four-cylinder HCCI engine. *IEEE T Contr Syst T* 2014; 22(3): 1190–1197.
23. Larimore J. *Experimental analysis and control of recompression homogeneous charge compression ignition combustion at the high cyclic variability limit*. PhD Dissertation, The University of Michigan, Ann Arbor, MI, 2014.
24. Morcinkowski B. *Simulative analyse von zyklischen Schwankungen der kontrollierten ottomotorischen Selbstzündung*. PhD Dissertation, RWTH Aachen University, Aachen, 2015.
25. Vaughan A. *Adaptive machine learning for modeling and control of non-stationary, near chaotic combustion in real-time*. PhD Dissertation, University of Michigan, Ann Arbor, MI, 2015.
26. Vaughan A and Bohac SV. A cycle-to-cycle method to predict HCCI combustion phasing. In: *ASME 2013 internal combustion engine division fall technical conference Volume 1: Large Bore Engines; Advanced Combustion; Emissions Control Systems; Instrumentation, Controls, and Hybrids*, Dearborn, Michigan, USA, 13–16 October, 2013. American Society of Mechanical Engineers, 2013, p.V001T03A026.
27. Ebrahimi K and Koch C. Model predictive control for combustion timing and load control in HCCI engines. SAE technical paper 2015-01-0822, 2015.
28. Choi S, Ki M and Min K. Development of an on-line model to predict the in-cylinder residual gas fraction by using the measured intake/exhaust and cylinder pressures. *Int J Automot Techn* 2010; 11(6): 773–781.
29. Pfluger J, Andert J, Ross H and Mertens F. Rapid control prototyping for cylinder pressure indication. *MTZ Worldwide* 2012; 73(11): 38–42.
30. Trajkovic S, Milosavljevic A, Tunestl P and Johansson B. FPGA controlled pneumatic variable valve actuation. SAE technical paper 2006-01-0041, 2006.
31. Wilhelmsson C, Tunestl P and Johansson B. FPGA based engine feedback control algorithms. In: *FISITA 2006 world automotive congress*. JSAE, 2006. http://lup.lub.lu.se/record/538193
32. Wick M, Lehrheuer B, Albin T, Andert J and Pischinger S. Decoupling of consecutive gasoline controlled autoignition combustion cycles by field programmable gate array based real-time cylinder pressure analysis. *Int J Engine Res* 2018; 19: 153–167.
33. Arora JK and Shahbakhti M. Real-time closed-loop control of a light-duty RCCI engine during transient operations. SAE technical paper 2017-01-0767, 2017.
34. Merker GP, Schwarz C and Teichmann R. Grundlagen Verbrennungsmotoren. In: *Simulation der Gemischbildung, Verbrennung, Schadstoffbildung und Aufladung*, vol. 4, 2009. Berlin, Germany: Springer-Verlag.

35. Pischinger R, Klell M and Sams T. *Thermodynamik der Verbrennungskraftmaschine*. Vienna: Springer-Verlag, 2009.
36. Woschni G. A universally applicable equation for the instantaneous heat transfer coefficient in the internal combustion engine. SAE technical paper 670931, 1967.
37. Chang J, Güralp O, Filipi Z, Assanis DN, Kuo T-W, Najt P and Rask R. New heat transfer correlation for an HCCI engine derived from measurements of instantaneous surface heat flux. SAE technical paper 2004-01-2996, 2004.
38. Hohenberg G. *Experimentelle Erfassung der Wandwärme von Kolbenmotoren*. PhD Thesis, University of Graz, Graz, 1980.
39. Soyhan H, Yasar H, Walmsley H, Head B, Kalghatgi G and Sorusbay C. Evaluation of heat transfer correlations for HCCI engine modeling. *Appl Therm Eng* 2009; 29(2–3): 541–549.
40. Wachtmeister PDIG. *Motordynamik und Brennverfahren*. 2012. Munich, Germany: Technical University of Munich.
41. Justi E. Die Dissoziation. In: *Spezifische Wärme Enthalpie, Entropie und Dissoziation technischer Gase*. New York: Springer, 1938, pp.123–141.
42. Zacharias F. *Analytische Darstellung der thermodynamischen Eigenschaften von Verbrennungsgasen*, 1966. Berlin, Germany: Technische Universitaet Berlin.
43. Heywood JB. *Internal combustion engine fundamentals*, vol. 930. New York: McGraw-Hill, 1988.
44. Van Basshuysen R and Schäfer F. *Handbuch Verbrennungsmotor: Grundlagen, Komponenten, Systeme, Perspektiven*. New York: Springer-Verlag, 2014.
45. Kronich A. *Methodik zur Entwicklung eines vollvariablen Ventiltriebes*. PhD Thesis, Technische Universität Kaiserslautern, Kaiserslautern, 2006.
46. Hauck S and DeHon A. *Reconfigurable computing: the theory and practice of FPGA-based computation*, vol. 1. Burlington, MA: Morgan Kaufmann, 2010.
47. Jung D and Assanis D. Multi-zone DI diesel spray combustion model for cycle simulation studies of engine performance and emissions. SAE technical paper 2001-01-1246, 2001.